CHEMISTRY
A EUROPEAN JOURNAL

DOI: 10.1002/chem.200700721

VIP

# Molecular Heterogeneous Catalysis: A Single-Site Zeolite-Supported Rhodium Complex for Acetylene Cyclotrimerization

**Philip W. Kletnieks,[a] Ann J. Liang,[b] Raluca Craciun,[c] Justin O. Ehresmann,[a] David M. Marcus,[a] Vinesh A. Bhirud,[b] Meghan M. Klaric,[a] Miranda J. Hayman,[a] Darryl R. Guenther,[a] Olesya P. Bagatchenko,[a] David A. Dixon,*[c] Bruce C. Gates,*[b] and James F. Haw*[a]**

**Abstract:** By anchoring metal complexes to supports, researchers have attempted to combine the high activity and selectivity of molecular homogeneous catalysis with the ease of separation and lack of corrosion of heterogeneous catalysis. However, the intrinsic nonuniformity of supports has limited attempts to make supported catalysts truly uniform. We report the synthesis and performance of such a catalyst, made from $[Rh(C_2H_4)_2(CH_3COCHCOCH_3)]$ and a crystalline support, dealuminated Y zeolite, giving $\{Rh(C_2H_4)_2\}$ groups anchored by bonds to two zeolite oxygen ions, with the structure determined by extended X-ray absorption fine structure (EXAFS) spectroscopy and the uniformity of the supported complex demonstrated by $^{13}C$ NMR spectroscopy. When the ethylene ligands are replaced by acetylene, catalytic cyclotrimerization to benzene ensues. Characterizing the working catalyst, we observed evidence of intermediates in the catalytic cycle by NMR spectroscopy. Calculations at the level of density functional theory confirmed the structure of the as-synthesized supported metal complex determined by EXAFS spectroscopy. With this structure as an anchor, we used the computational results to elucidate the catalytic cycle (including transition states), finding results in agreement with the NMR spectra.

**Keywords:** alkynes · cyclotrimerization · heterogeneous catalysis · rhodium · supported catalysts · zeolites

## Introduction

Solid catalysts offer decisive technological advantages over fluids, being noncorrosive and easily separated from fluid products. However, most solid catalysts are unselective, because their intrinsically nonuniform surfaces present active sites with a spectrum of activities. Elucidation of the structures and reactivities of these sites is challenging, because of nonuniformity and because they are small and dispersed. In contrast, homogeneous catalysis, although generally lacking the aforementioned advantages of heterogeneous catalysis, may be economically attractive when the catalysts are highly selective; selectivity is often associated with the uniformity of the molecular catalytic species.[1] Supported catalysts[2] could offer the advantages of both solid and soluble catalysts if they could be made to be essentially uniform; this would require nearly uniform supports and nearly uniform sites anchored to them.

We have prepared a uniform supported-catalyst precursor by using a crystalline support (a zeolite) to which a rhodium complex was bonded; this metal complex has reactive ethyl-

[a] P. W. Kletnieks, Dr. J. O. Ehresmann, Dr. D. M. Marcus, M. M. Klaric, M. J. Hayman, D. R. Guenther, O. P. Bagatchenko, Prof. J. F. Haw
Department of Chemistry
University of Southern California
Los Angeles, CA 90089 (USA)
Fax: (+1) 213-740-2701
E-mail: jhaw@usc.edu

[b] A. J. Liang, Dr. V. A. Bhirud, Prof. B. C. Gates
Department of Chemical Engineering and Materials Science
University of California, One Shields Ave.
Davis, CA, 95616 (USA)
Fax: (+1) 530-752-1031
E-mail: bcgates@ucdavis.edu

[c] R. Craciun, Prof. D. A. Dixon
Department of Chemistry, University of Alabama
Tuscaloosa, AL, 35487 (USA)
Fax: (+1) 205-348-4704
E-mail: dadixon@bama.ua.edu

Supporting information for this article is available on the WWW under http://www.chemeurj.org/ or from the author.

ene ligands, allowing facile entry into catalytic cycles including olefin hydrogenation. The ethylene ligands in the supported complex exhibit the uniform fluxionality of molecular species, as shown by $^{13}C$ MAS NMR spectra reported in a recent communication.[3]

We now report a full characterization of this catalyst for acetylene trimerization, combining spectroscopic results with calculations at the density functional theory (DFT) level to determine the catalytic cycle, including transition states. The results characterizing the supported catalyst demonstrate a depth of understanding rivaling that of well-understood examples of homogenous catalysis.

## Results

The supported metal complex was formed by the reaction of $[Rh(C_2H_4)_2(acac)]$ (acac = $CH_3COCHCOCH_3$) with dealuminated Y zeolite and characterized by IR, $^{13}C$ NMR, and EXAFS (extended X-ray absorption fine structure) spectroscopy as well as by density functional theory; the results demonstrate that it is a site-isolated rhodium complex with two π-bonded ethylene ligands that is bound to two oxygen atoms of the support. When hydrogen flowed over this supported complex, ethane was formed; when ethylene and hydrogen flowed over the complex together at 1 bar and 294 K, catalytic hydrogenation to form ethane occurred.[4] Our results also show that propylene was catalytically hydrogenated in the presence of $H_2$ to give propane, with no evidence of deactivation after 20 turnovers. GC-FID and GC-MS analysis of the product stream confirmed the displacement of ethylene from the catalyst by the first two propylene pulses; conversion of propylene to propane was quantitative. In separate experiments, the number of turnovers was measured in a once-through flow reactor with continuously fed propylene + $H_2$; the value was found to be 120 after 14 h, and the catalyst had not undergone measurable deactivation when the experiment was stopped.

Not surprisingly, the intermediates in these cycles were not spectroscopically observable (although such intermediates have been observed on supported metal clusters[5]). Thus, without a basis for elucidation of the catalytic cycles, we turned to another well-investigated catalytic test reaction that involves small reactant and product molecules, namely, acetylene cyclotrimerization to form benzene.

The initial pulse of acetylene into a flow reactor containing the as-synthesized sample (designated as the precursor, **PRE**) resulted in the formation of gas-phase benzene along with ethylene displaced from **PRE** as it was converted in the catalytic cycle. Subsequent pulses continued to form benzene, albeit with a progressive deactivation of the catalyst, with the final number of turnovers being eight (on the basis of the number of benzene molecules formed per $Rh^+$ present).

The results presented below show that this reaction offers a unique opportunity for the observation of intermediates in a catalytic cycle analogous to those observed previously in homogeneous catalysis and in gas-phase investigations of model homogeneous catalytic processes.[6]

Figure 1 is a schematic representation of the catalytic cycle determined on the basis of our computations for the conversion of acetylene on the supported catalyst, with the structures of the intermediates and a summary of the characterization methods used to identify each species, including **PRE**. In the synthesis of **PRE** from $[Rh(C_2H_4)_2(acac)]$, the anionic ligand acac is replaced by an anionic site of the support (near one of the zeolite Al ions). Subsequent replacement of the ethylene ligands of **PRE** with acetylene initiates the catalytic cycle. IR spectra confirmed the removal of the acac ligand and the presence of ethylene ligands on the anchored rhodium complex **PRE**. The C–H stretching peak at 3073 $cm^{-1}$, associated with benzene bonded to Rh centers,[7] appeared in the IR spectra after the sample had been brought in contact with acetylene to form a benzene complex of rhodium on the support.

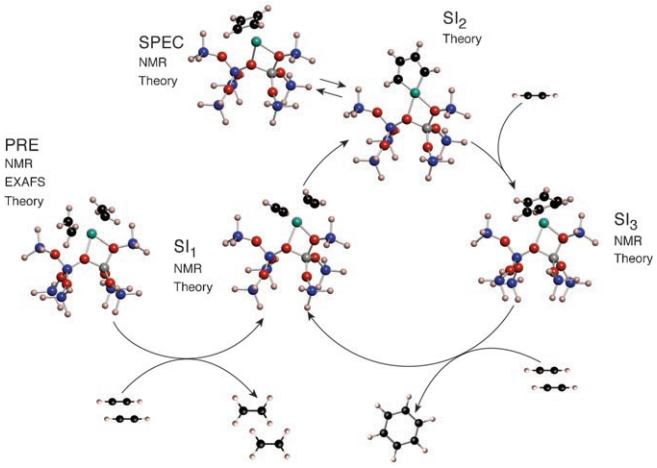


Figure 1. Catalytic cycle for cyclotrimerization of acetylene catalyzed by a single-site $Rh^+$ center bonded to a zeolite support by two Rh–O bonds. The reactive organic groups bonded to Rh in the as-synthesized catalyst (at left, **PRE**), two ethylenes, allow facile entry into a catalytic cycle. **PRE** has been characterized by EXAFS and $^{13}C$ NMR spectroscopies as well as density functional theory. (Characterization methods for all the species are shown on the figure.) When the sample is brought in contact with gas-phase acetylene, the ethylene is replaced by acetylene, to form the stable intermediate $\mathbf{SI_1}$, initiating the catalytic cycle. This intermediate undergoes ring closure via transition state $\mathbf{TS_{1\rightarrow 2}}$, forming the metallacycle $\mathbf{SI_2}$, which equilibrates with the more stable cyclobutadiene complex (**SPEC**, a spectator species). The pool consisting of $\mathbf{SI_2}$ and **SPEC** crosses via transition state $\mathbf{TS_{2\rightarrow 3}}$ into the stable benzene complex $\mathbf{SI_3}$. Dissociation of product benzene into the gas phase, compensated by adsorption of reactant acetylene, closes the cycle.

**Identification of hydrocarbon ligands on Rh by $^{13}C$ NMR spectroscopy**: Of the significant intermediates along the reaction pathway, two ($\mathbf{SI_1}$ and $\mathbf{SI_3}$) have been observed by solid-state NMR spectroscopy (Figure 2) with their assignments as the bis-acetylene and benzene complexes, in agreement with $^{13}C$ shift for analogous solution complexes. The third intermediate ($\mathbf{SI_2}$) has been inferred, on the basis of

  

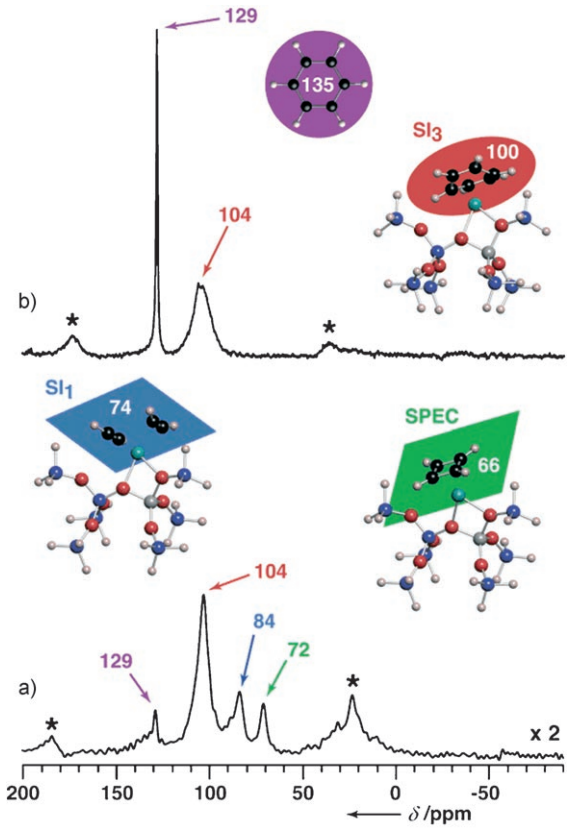


Figure 2. $^{13}C$ MAS NMR spectra of the zeolite-supported $Rh^+$ ion sampling two distributions of the species over the catalytic cycle of Figure 1. a) Entering the cycle by exchanging [$^{13}C_2$]actelylene for the unlabeled ethylene ligands in **PRE** leads to $\mathbf{SI_1}$ (84 vs. 74 ppm theoretical), **SPEC** (72 vs. 66 ppm theoretical), $\mathbf{SI_3}$ (104 vs. 100 ppm theoretical), and product, free benzene (129 vs. 135 ppm theoretical). b) Entering the cycle by displacing unlabeled ethylene ligands with excess [$^{13}C_6$]benzene leads to $\mathbf{SI_3}$ directly, and decyclotrimerization to preceding parts of the cycle is essentially precluded by thermodynamics (vide infra). The symbol * denotes rotational sidebands. Theoretical chemical shift values were computed by using the GIAO formalism with the B3LYP exchange-correlation functional with the Stuttgart effective core potential (ECP) basis set on Rh and a polarized triple zeta basis set on the other atoms. The calculated geometries are shown in the figure.

DFT calculations, to be in equilibrium with a structurally related spectator cyclobutadiene complex (**SPEC**) that we also observed by $^{13}C$ solid-state NMR spectroscopy, as shown in Figure 2. The benzene complex $\mathbf{SI_3}$ was characterized by NMR spectroscopy after entering the cycle in either the forward direction, by exchange of **PRE** with acetylene-$^{13}C_2$, or the reverse direction, by exchange with benzene-$^{13}C_6$.

The spectral assignments shown in Figure 2 were made in part on the basis of comparisons with results of reported NMR characterizations of analogous rhodium compounds in solution,[8] as shown in Scheme 1. Lacking data for a reference compound providing a more exact match to the bis-acetylene Rh complex, we selected the related complex **1** (Scheme 1). The ethyl propiolate ligand in **1**, which has an unsubstituted acetylenic carbon atom, is used for comparison with our supported complex incorporating two acetylene ligands, $\mathbf{SI_1}$. The $^{13}C$ chemical shift characterizing acetylene

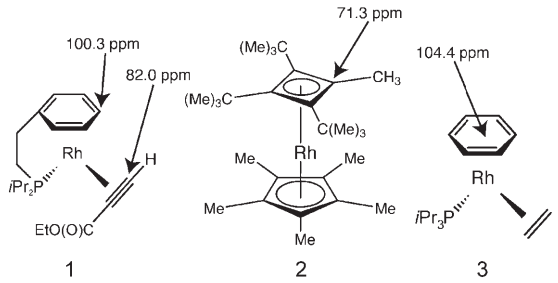


Scheme 1. Compounds of $Rh^+$ with assignments of $^{13}C$ solution NMR resonances, providing a basis for the assignments shown in Figure 2.

is only slightly upfield of the corresponding shift characterizing $sp^3$ carbon atoms in ethyl propiolate. Further interpretation of the $^{13}C$ NMR assignments is made on the basis of our DFT calculations (vide infra).

**Structural characterization of supported rhodium precursor complex by EXAFS spectroscopy**: The supported rhodium complex (**PRE**) prepared from [$Rh(C_2H_4)_2(acac)$] was characterized by Rh K-edge (23,220 eV) EXAFS spectroscopy. Data were communicated previously,[3,4] and we now report a complete analysis of results on the basis of newly measured data of higher quality; the results essentially match those previously communicated.[3,4]

EXAFS data characterizing **PRE** are shown in Figure 3. The initial data fitting with the plausible absorber–backscatterer contributions (Rh–O, Rh–C, Rh–Rh, and Rh–Al) led to a narrowed list of candidate fits (models), based on the goodness of fit. We continued to include an Rh–Rh contribution although the initial analysis gave no indication of such a contribution, because of the ease of reduction and potential for aggregation of rhodium in complexes on oxide supports.[9] The fits carried out in the most detail are summarized in Table 1. No fit with only two shells (contributions) was adequate.

Each of the six models includes both Rh–C and Rh–O contributions, consistent with the presence of ethylene ligands (as demonstrated by the IR and $^{13}C$ NMR spectra) and Rh–support oxygen bonds anchoring the metal complex to the zeolite. The six models differ from each other with respect to the Rh–Rh contribution and other Rh–support contributions, that is, Rh–Al and a second Rh–O contribution.

Besides the Rh–C and Rh–O contributions, the three-shell model I (Table 1) includes a second Rh–O contribution, model II includes an Rh–Al contribution, and model III includes an Rh–Rh contribution. Similarly, in addition to the Rh–C and Rh–O contributions, the four-shell model IV includes a second Rh–O contribution and an Rh–Al contribution, model V includes a second Rh–O contribution and a Rh–Rh contribution, and model VI includes a Rh–Al contribution and a Rh–Rh contribution. Details of the fits with all these models are given in Supporting Information.

All the models except III, V, and VI, each of which includes an Rh–Rh contribution, fit the data well, with the quality of the fit varying slightly from one to another.

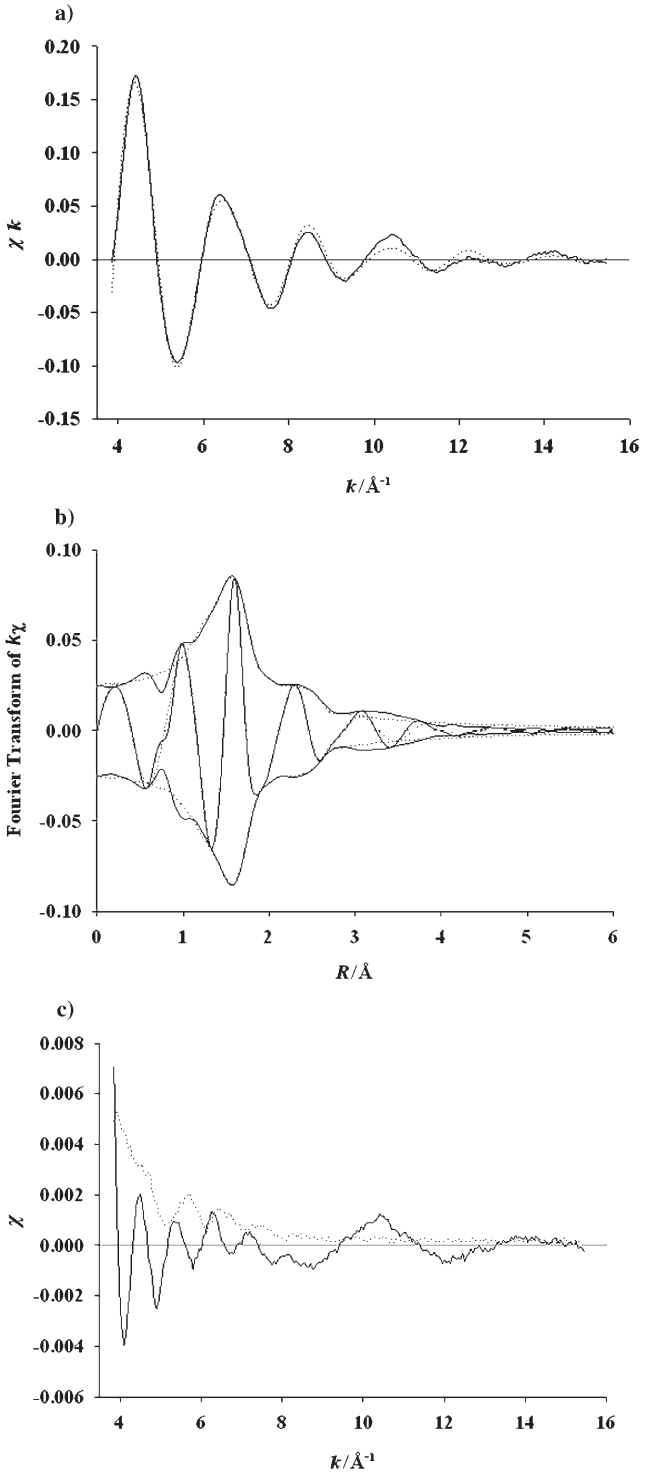


Figure 3. a) Results of EXAFS data analysis for the as-synthesized sample **PRE**: EXAFS function $\chi$ (solid line) with $k^1$-weighted and calculated contributions (dotted line) corresponding to the structural parameters reported (model II). b) Results of EXAFS data analysis for **PRE**. Shown here are the imaginary part and the magnitude of the Fourier transform of the raw data (solid line) (in $k^1$-weighting) and calculated contributions (dotted line) corresponding to the structural parameters reported. c) Standard deviations in the EXAFS function ($\chi$ function) and the residuals of the model fit from the data for the sample corresponding to **PRE**. Solid line, standard deviations for each of the data points calculated with the software XDAP; dotted line, residuals remaining when the sum of the calculated contributions (to the $\chi$ file) were subtracted from the raw data.

Models II and IV fit the data best, and model V provides the worst fit; details are given in Table 2, in which the values of the fit diagnostic parameters, $\varepsilon_v^2$ (goodness of fit) and the variances between the data and postulated models for the EXAFS function $\chi$ and the Fourier transform of $\chi$ are summarized.

Model IV differs from model II by the inclusion of a new contribution, a second Rh–O contribution (Rh–$O_l$, the subscript refers to long); addition of the new contribution led to essentially no improvement in the overall fit and to essentially no change in the values of the parameters characterizing the three contributions common to the two models (Rh–O, Rh–C, and Rh–Al) within the error of the analysis. Instead, the additional contribution added uncertainty in the fit; furthermore, the Debye–Waller factor characterizing the Rh–Al contribution is relatively large ($9.1\times10^{-3}$ Å$^2$), with an uncertainty of $13\times10^{-3}$ Å$^2$, and thus is of doubtful physical significance (nor could it be distinguished from a Rh–Si contribution).

Model I provides a good overall fit; however, the shell characterizing the Rh–$O_l$ contribution was found not to fit well after the contribution was corrected for phase and amplitude.

Each of the models III, V, and VI includes a Rh–Rh contribution; addition of this contribution to the simpler models did not improve the fits substantially. In the three-shell model III, besides the Rh–O and Rh–C contributions, a small Rh–Rh contribution was determined, with an Rh–Rh distance of 2.60 Å and a coordination number less than 0.2. This contribution enhanced the overall fit slightly compared with the model including only two contributions; however, the individual Rh–Rh shell was found not to fit the data well after the contribution was corrected for phase and amplitude (Supporting Information). Similarly, in the four-shell models V and VI, the individual Rh–Rh shell was found not to fit the data well after the contribution was corrected for phase and amplitude. Furthermore, the Debye–Waller factor representing this contribution in model V is also relatively large, $13\times10^{-3}$ Å$^2$ (with an uncertainty of $1.4\times10^{-3}$ Å$^2$).[10,11]

In summary, the added contributions to generate four-shell models did not enhance the overall fits significantly. Although the combination of the two contributions (Rh–$O_s$ and Rh–C; s refers to short) that are common to all of the models does not provide an adequate overall fit by itself, and the additional contribution (or contributions) does (or do) improve the overall fit, none of the additional contributions (when corrected for phase and amplitude) gives a satisfactory fit of the individual shell. Of the six models, the three-shell model II (with Rh–O, Rh–C, and Rh–Al contributions) is the one that fits the data best with physically realistic parameters.

According to this model, the supported as-synthesized sample **PRE** is a mononuclear rhodium–diethylene complex with 1) two Rh–O bonds, at a distance of 2.14 Å, which matches the metal–oxygen distances in numerous compounds of $Rh^+$ and in numerous oxide- and zeolite-support-

  

Table 1. Qualitative summary of EXAFS fitting results for six candidate models representing the supported as-synthesized complex **PRE**.

| Model | Absorber/ backscatterer contributions | Comments regarding the quality of fit of EXAFS data |
|---|---|---|
| I | Rh–$O_s$[a] | adequate overall fit; |
| | Rh–C | physically realistic values of all parameters; |
| | Rh–$O_l$[b] | individual Rh–$O_l$ shell not well fitted when phase- and amplitude-correction applied |
| II | Rh–$O_s$[a] | good overall fit, better than model I; |
| | Rh–C | physically realistic values of all parameters; |
| | Rh–Al | parameters characterizing Rh–$O_s$ and Rh–C almost the same as those determined for model I |
| III | Rh–$O_s$[a] | good overall fit (as shown by goodness of fit parameters), but |
| | Rh–C | comparison of fit with data (Supporting Information) indicates less than adequate fit; |
| | Rh–Rh | physically realistic values of all parameters; Rh–Rh contribution small (coordination number $\approx$0.2, Rh–Rh distance = 2.6 Å) and individual Rh–Rh shell not well fitted when phase- and amplitude-corrections applied |
| IV | Rh–$O_s$[a] | good overall fit, similar to that of model II; |
| | Rh–C | physically realistic values of all parameters; |
| | Rh–$O_l$[b] | addition of Rh–$O_l$ contribution give no improvement to overall fit |
| | Rh–Al | relative to model II; parameters characterizing Rh–$O_s$ and Rh–C almost the same as those determined for model II; individual Rh–$O_l$ and Rh–Al shells not well fitted when phase- and amplitude-corrections applied |
| V | Rh–$O_s$[a] | unsatisfactory overall fit; |
| | Rh–C | individual Rh–Rh shell not well fitted when phase- and amplitude- |
| | Rh–$O_l$[b] | correction applied (Rh–Rh coordination number $\approx$0.7, with short Rh–Rh bonding distance of 2.57 Å and large Debye-Waller |
| | Rh–Rh | factor of $12.7\times10^{-3}$ Å$^2$) |
| VI | Rh–$O_s$[a] | adequate overall fit; |
| | Rh–C | individual Rh–Rh shell not well fitted when phase- and amplitude-correction applied |
| | Rh–Al | (Rh–Rh coordination number $\approx$0.2, with short Rh–Rh bonding distance of 2.53 Å); |
| | Rh–Rh | errors associated with $\Delta E_0$ for Rh–Rh and Rh–Al contributions very large ($>\pm100$%) |

[a] Rh–$O_s$ is a short Rh–O contribution, with oxygen being part of the support and the distance being a bonding distance. [b] Rh–$O_l$ is a longer (non-bonding) distance.

Table 2. Fit Diagnostic Parameters for the EXAFS Models representing the Supported Precursor **PRE**.

| | Model I | | | | Model II | | | | Model III | | | |
|---|---|---|---|---|---|---|---|---|---|---|---|---|
| $\Delta k$ [Å$^{-1}$] | 3.85–15.46 | | | | 3.85–15.46 | | | | 3.85–15.46 | | | |
| $\Delta r$ [Å] | 1.00–4.00 | | | | 1.00–4.00 | | | | 1.00–4.00 | | | |
| $\varepsilon_v^2$ | 11.2 | | | | 7.0 | | | | 10.1 | | | |
| | $k^0$ | $k^1$ | $k^2$ | $k^3$ | $k^0$ | $k^1$ | $k^2$ | $k^3$ | $k^0$ | $k^1$ | $k^2$ | $k^3$ |
| $\chi$ variance | 1.71 | 2.11 | 4.75 | 13.0 | 1.06 | 1.62 | 4.32 | 12.5 | 1.53 | 2.19 | 5.01 | 13.2 |
| FT Im part variance | 0.47 | 0.72 | 1.85 | 5.16 | 0.31 | 0.63 | 1.79 | 5.10 | 0.48 | 0.86 | 2.08 | 5.26 |
| FT Re part variance | 0.91 | 1.58 | 4.30 | 12.2 | 0.72 | 1.37 | 4.01 | 11.7 | 1.16 | 1.92 | 4.70 | 12.4 |
| | Model IV | | | | Model V | | | | Model VI | | | |
| $\Delta k$ [Å$^{-1}$] | 3.85–15.46 | | | | 3.85–15.46 | | | | 3.85–15.46 | | | |
| $\Delta r$ [Å] | 1.00–4.00 | | | | 1.00–4.00 | | | | 1.00–4.00 | | | |
| $\varepsilon_v^2$ | 10.5 | | | | 13.1 | | | | 11.5 | | | |
| | $k^0$ | $k^1$ | $k^2$ | $k^3$ | $k^0$ | $k^1$ | $k^2$ | $k^3$ | $k^0$ | $k^1$ | $k^2$ | $k^3$ |
| $\chi$ variance | 1.06 | 1.60 | 4.24 | 12.3 | 1.34 | 1.82 | 4.46 | 12.6 | 1.01 | 1.69 | 4.11 | 12.3 |
| FT Im part variance | 0.30 | 0.61 | 1.75 | 5.03 | 0.33 | 0.65 | 1.82 | 5.22 | 0.33 | 0.63 | 1.74 | 4.95 |
| FT Re part variance | 0.67 | 1.32 | 3.92 | 11.5 | 0.71 | 1.39 | 4.06 | 11.8 | 0.76 | 1.39 | 3.80 | 11.5 |

ed metal complexes;[13] 2) four Rh–C bonds with a distance of 2.05 Å, slightly smaller than the distances in rhodium–ethylene complexes such as [Rh($C_2H_4$)$_2$(acac)] (2.13 Å[14]); and 3) a Rh–Al contribution with a coordination number of 1.0 at a distance of 2.95 Å. The Rh–O coordination number demonstrates that the zeolite is a bidentate ligand; the Rh–C coordination number indicates two ethylene ligands per Rh atom; and the Rh–Al coordination number indicates bonding of the cationic rhodium complex in the zeolite at the expected anionic site. The fact that the zeolite acts as a bidentate ligand is consistent with binding of the $Rh^+$ in the negatively charged sites in the zeolite in which Al is present in the lattice rather than Si.

We emphasize that this structure is confirmed by the previously reported $^{13}$C NMR data, which demonstrated the high degree of uniformity of the supported complexes.[3]

**Density functional theoretical modeling of the supported as-synthesized rhodium complex and the catalytic acetylene trimerization cycle**: Our modeling of **PRE** and the catalytic

  

cycle for acetylene cyclotrimerization began with an examination of the thermodynamics of the critical species involved in the trimerization reaction. The calculated trimerization energy of three acetylene molecules to form one benzene molecule is predicted to be 149.5 kcal mol$^{-1}$; for comparison, the experimental trimerization energy is 142.8 kcal mol$^{-1}$.[15] In the following subsections, we describe the models of the zeolite and the catalytic species used in the calculations, then present a comparison of the EXAFS data and model of **PRE** with the calculated results as well as a comparison of NMR results characterizing reaction intermediates with calculated results.

*Models of rhodium complex and bonding site in zeolite*: The supported rhodium complexes, including the as-synthesized sample **PRE** and intermediates in the acetylene trimerization cycle, were investigated with the reactants bonded to 1) a naked $Rh^+$ ion, 2) a $Rh^+$ ion bonded to the site in the zeolite represented as an $Al(OH)_4^-$ species (thus forming the neutral $Al(OH)_4Rh$), and 3) in calculations with the most stable supported rhodium complexes, a cluster of the zeolite incorporating 8T (Si+Al) atoms (as depicted in Figure 2).

Because the ground state of the atom is a triplet, both the lowest lying singlet (Figure 4) and triplet energy surfaces (Figure 5) characterizing $Rh^+$ and $Al(OH)_4Rh$ were investigated. The singlet–triplet splittings are shown in Table 3. The triplet state is predicted to be the ground state of the $Rh^+$ ion, as found experimentally.[16]

The calculations predict that triplet $Rh^+$ is more stable than singlet $Rh^+$ when bound to the model of the zeolite site ($Al(OH)_4^-$; Table 3), although bonding of the $Rh^+$ ion to this site substantially reduces the singlet–triplet splitting. Addition of acetylene to either the naked ion or this site results in a substantial stabilization of the singlet, so that when two acetylene molecules are π bonded to the $Rh^+$, the singlet is stabilized (and stabilization of the singlet occurs with the addition of just one acetylene molecule). Rearrangement of the acetylenes to form the $C_4H_4$ and $C_6H_6$ species on the naked-ion potential-energy surface leads to an increase in the stabilization of the triplet, so that for the atomic ion and the ion bonded to the model zeolite site, the singlet and triplet are approximately degenerate for the $RhC_4H_4^+$ (**$SI_2$**) species. The formation of benzene on the atomic ion leads to the triplet becoming more stable, but when the complex is present on the site, the singlet is more stable, consistent with our being able to observe an NMR spectrum of the benzene complexed to the rhodium. We emphasize that we generate the catalytic site by substituting the acac in $[Rh(C_2H_2)_2(acac)]$ with the zeolite site near the Al ion. The singlet–triplet splitting in the acac is 24.5 kcal mol$^{-1}$, favoring the singlet. Thus, exchange of the acac ligand for the bidentate zeolite site will initially form the singlet in the supported catalyst, and the catalytic reaction is expected to proceed on the singlet surface if no singlet–triplet crossings occur.

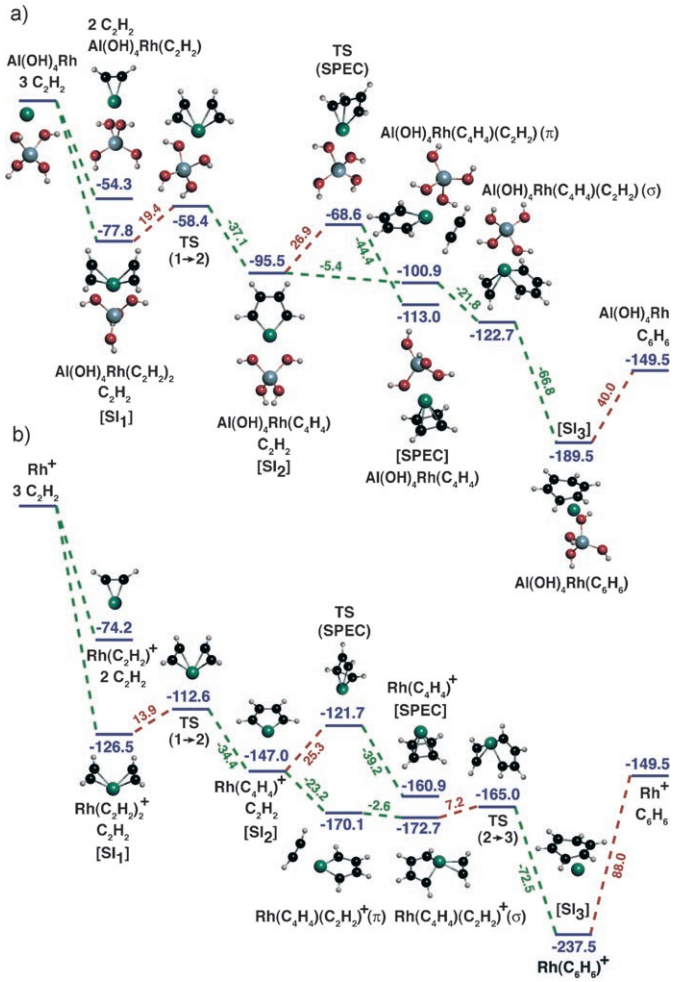


Figure 4. Detailed descriptions of the theoretical potential energy surfaces for acetylene cyclotrimerization catalysis by a) supported $Rh^+$ ion in a zeolite modeled as $RhAlO_4H_4$ and b) gas-phase $Rh^+$ ion. The surface is always with respect to the asymptote of $Rh^+ + 3C_2H_2$ or $Al(OH)_4Rh + 3C_2H_2$. Some of the acetylene molecules relative to the asymptote are not shown for clarity. When molecules are shown on a second line, they are not bonded to the catalytic site and are part of the asymptotic energy. The reaction steps and barrier heights are essentially identical for the gas-phase metal ion catalyst and its supported analogue. In addition to the stable intermediates shown in the other figures, we also found two structures in which the third acetylene binds to metallacycle **$SI_2$**, but the barrier for conversion of this to **$SI_3$** was very small in the gas phase and so small for the supported catalyst that the state could not even be found. In each case the singlet surfaces are shown. The triplet surfaces are shown in Figure 5. Many of the states, especially for the supported catalyst, are more stable as singlets, and this result is reflected in our ability to observe these by NMR spectroscopy. Energies including zero-point effects are reported in kcal mol$^{-1}$ and were calculated with the B3LYP level exchange-correlation functional and the Stuttgart/ECP basis sets on Rh and the aug//cc-pVDZ on the other atoms.

*Comparison of EXAFS data and DFT calculations representing the as-synthesized catalyst **PRE***: Table 4 gives a summary of the EXAFS structural parameters characterizing **PRE** and the DFT results characterizing this species for the two models of the zeolite site mentioned above. The experimental Rh–O coordination number is 1.6, which, within the estimated error of the measurement (approximately ±20%;

  

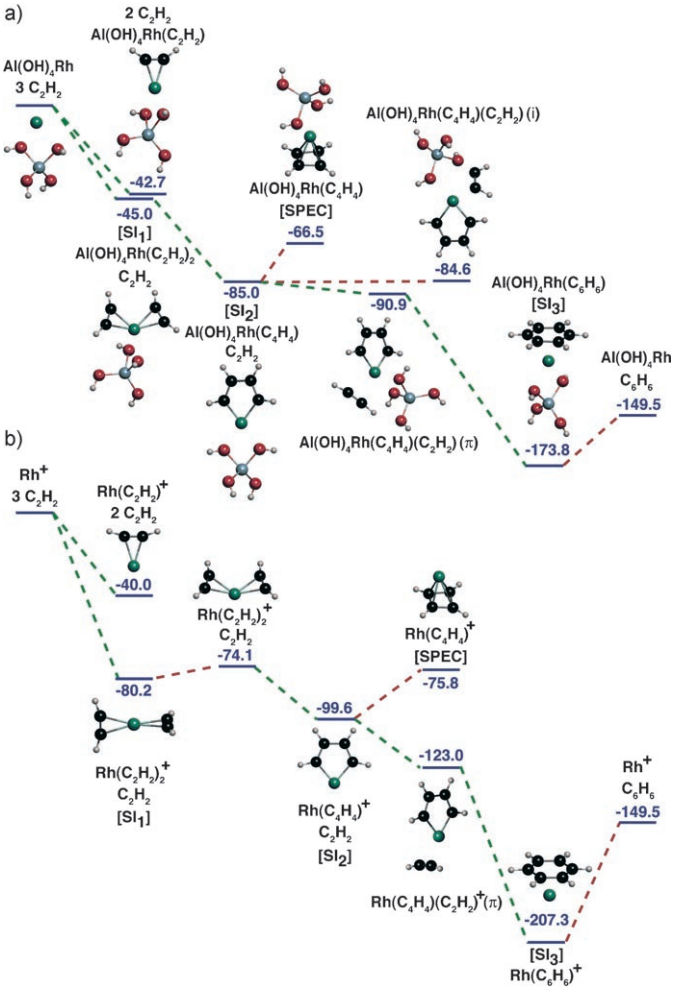


Figure 5. Theoretical potential-energy surfaces characterizing the triplet potential energy surface for acetylene cyclotrimerization catalysis by a) supported $Rh^+$ ion modeled as $Al(OH)_4Rh$ and b) gas-phase $Rh^+$ ion. Energies are given in kcal mol$^{-1}$. The triplet surfaces are shown for comparison with the very similar singlet surfaces shown in Figure 4.

Table 3. Singlet–triplet energy splittings in kcal mol$^{-1}$ for various $Rh^+$ species.[a]

| Gas-phase ion | $\Delta E_{ST}$ | Zeolite model | $\Delta E_{ST}$ |
|---|---|---|---|
| $Rh^+$ | 47.6 | $Al(OH)_4Rh$ | 11.3 |
| $RhC_2H_2^+$ | 13.4 | $Al(OH)_4RhC_2H_2$ | −0.2 |
| $Rh(C_2H_2)_2^+$ (**SI$_1$**) | −4.7 | $Al(OH)_4Rh(C_2H_2)_2$ (**SI$_1$**) | −21.4 |
| $RhC_4H_4^+$ (**SI$_2$**) | 0.2 | $Al(OH)_4RhC_4H_4$ (**SI$_2$**) | 0.9 |
| $RhC_4H_4^+$ (**SPEC**) | −37.5 | $Al(OH)_4RhC_4H_4$ (**SPEC**) | −35.2 |
| $RhC_4H_4C_2H_2^+$ (π) | 0.5 | $Al(OH)_4RhC_4H_4C_2H_2^+$ (π) | 1.3 |
| $RhC_6H_6^+$ (**SI$_3$**) | 17.4 | $Al(OH)_4RhC_6H_6$ (**SI$_3$**) | −4.3 |

[a] Calculated at the B3LYP level with the aug//cc-pVDZ and the Stuttgart/ECP basis sets including zero-point effects. Whereas the overall shapes of the singlet and triplet surfaces are very similar, supporting the catalyst has the effect of stabilizing the singlet states for many of the stable species. Positive values of $\Delta E_{ST}$ mean that the triplet is more stable.

this statement of error represents the accuracy rather than the precision, as in the remainder of this paragraph), essentially matches the value of 2 from the calculations with the zeolite being a bidentate ligand. The Rh–O bond length determined by EXAFS spectroscopy is $2.14 \pm 0.02$ Å, in satisfactory agreement with the DFT values of 2.12 and 2.17 Å for the two models of the zeolite site (Table 4). The Rh–C coordination number was determined experimentally to be $3.9 \pm 20\,\%$, as expected for two ethylene ligands π bonded to Rh. The calculations show two ethylenes equally bonded to the Rh for a coordination number of four. The Rh–C bond length determined by the EXAFS data was found to be $2.05 \pm 0.02$ Å. The calculated values of 2.13 and 2.12 Å (Table 4) are longer.

Table 4. Structural parameters corresponding to best fit of EXAFS data characterizing the as-synthesized catalyst **PRE** (model II) and comparison with calculated results.[a]

| | EXAFS | | | | DFT | | |
|---|---|---|---|---|---|---|---|
| Shell | $N$ | $R$ [Å] | $10^3 \times \Delta\sigma^2$ [Å$^2$] | $\Delta E_0$ [eV] | $N$ | $R$ [Å][b] | $R$ [Å][c] |
| Rh–Rh | [d] | | | | | | |
| Rh–O$_s$ | 1.6 | 2.14 | 2.4 | 0.7 | 2.0 | 2.12 | 2.17 |
| Rh–C | 3.9 | 2.05 | 2.3 | 0.7 | 4.0 | 2.13 | 2.12 |
| Rh–Al | 1.0 | 2.95 | 7.8 | 13 | 1.0 | 2.99 | 2.89 |

[a] Abbreviations: $N$, coordination number; $R$, absorber-scatterer distance; $\Delta\sigma^2$, Debye-Waller factor; and $\Delta E_0$, inner potential correction; L denotes ligand; the subscripts s and l refer to short and long, respectively. [b] Calculated in model $Rh(L)_xAl(OH)_4$. [c] Calculated in model incorporating 8T atoms. [d] Contribution not detectable.

To benchmark the DFT method, we also calculated the structure of $[Rh(C_2H_4)_2(acac)]$. The calculated bond lengths are 2.148 Å for the Rh–C($C_2H_4$) distance and 2.071 Å for the Rh–O distance, as compared to the experimental values for Rh–C and Rh–O of 2.13 and 2.05 Å from the X-ray crystal structure of the precursor $[Rh(C_2H_4)_2(acac)]$.[23] This comparison shows that we would expect the calculated bond lengths in the model of the zeolite to be a bit too long, consistent with the tendency of DFT to predict values that are too long for such donor–acceptor complexes.[17] The Rh–Al coordination number was determined to be 1 (with an error $> \pm 0.2$), consistent with the presence of one cationic rhodium complex per site. The calculated values of 2.99 and 2.89 Å for the Rh–Al distance are in satisfactory agreement with EXAFS value of 2.95 Å (with an error of more than $\pm 0.02$ Å).

*Comparison of NMR results with DFT calculations*: The DFT calculations of the intermediates and spectator in the catalytic cycle (Figure 1) aid in the interpretation of the chemical shift assignments. **PRE** and the spectator species **SPEC** in the catalytic cycle were represented by the two models of the zeolite site described above (Figure 2). Chemical shift values were calculated for comparison with experiment with the resultant differences ranging from 4 to 10 ppm. The calculations confirmed that all the species that had been characterized by NMR spectroscopy (**PRE**, **SI$_1$**, **SI$_3$**, and **SPEC**) are ground-state singlets and, on the basis of the energetics, should accumulate at analytically useful equilibrium concentrations at moderate temperatures. The calculations also show that the one significant intermediate

not observed by NMR spectroscopy ($\mathbf{SI_2}$) is predicted to be a ground-state triplet by 0.9 kcal mol$^{-1}$ (Table 3). Intermediate $\mathbf{SI_2}$ readily reacts with acetylene to from benzene on the singlet potential surface (Figure 4), so that it would be present at a negligible equilibrium concentration during catalysis. The spectator complex **SPEC**, on the other hand, does not readily react with additional acetylene to form benzene on the singlet surface, and this result shows why it can be observed as an intermediate. Because the reaction is initiated on the singlet potential-energy surface and the various singlet species are energetically accessible as singlets, there is no need to invoke singlet–triplet crossing. We note that the presence of the second-row transition-metal atom would aid singlet–triplet crossing for species with small singlet–triplet splittings, such as that predicted for $\mathbf{SI_2}$, for which the singlet and triplet are within 1 kcal mol$^{-1}$ of each other.

## Discussion

**Acetylene cyclotrimerization catalysis in various phases**: The overall catalytic cycle shown in Figures 1, 4, and 5 is qualitatively in agreement with previous models of the cyclotrimerization reaction in solution catalyzed by $[CoCp]^+$ [18] and various $Co^+$, $Rh^+$, and $Ir^+$ complexes.[19] Our results can also be compared with those of Wesendrup and Schwarz,[6] who used ion-cyclotron resonance spectroscopy to investigate benzene formation in the gas-phase catalytic reactions of cyclobutadiene and acetylene with complexes of $Rh^+$ and of $Ru^+$. These authors determined the reactivity of the $C_4H_4$ complex of $Rh^+$ with acetylene, finding that the catalytic cycle turned over six times as $[MC_4H_4]^+$ reacted with acetylene to form free benzene and bare $Rh^+$. Ion-molecule collision experiments established that $RhC_4H_4^+$ was a key intermediate, most likely present as a cyclobutadiene complex rather than a metallacycle, although the latter cannot be ruled out on the basis of the experimental results. Results characterizing the products of the gas-phase ion–molecule reaction indicate that it most likely takes place on the triplet surface, corresponding to the most stable metal-ion spin state. The data reported by Wesendrup and Schwarz[6] are consistent with our calculated potential-energy surfaces.

Our calculations show that the bonding of the hydrocarbon ligands is not significantly affected by the presence of the zeolite support, as the benzene complexes with the bare atomic ion and with the rhodium complex incorporating the zeolite as a ligand are characterized by similar bonding of the benzene, which is predicted to bind $\eta^2$ to $\eta^4$ in each. Thus, there are similarities between the gas-phase cyclotrimerization reaction in the presence of $Rh^+$ and in the presence of our isolated zeolite-bound surface site, although we note that there may be differences in the spin states that may control the reactivity.

**Comparison of NMR results and theoretical catalytic cycle**: The results presented here provide some direct comparisons of NMR spectra of catalytic intermediates and the calculated results characterizing the catalytic cycle. On the NMR timescale, the six carbon atoms in the benzene bonded to the Rh atom are all equivalent, with a single $^{13}C$ resonance for $\mathbf{SI_3}$. The average of the six theoretical values (ranging from 68 to 148 ppm) is 100 ppm, in good agreement with the experimental value of 104 ppm. The difference is consistent with the difference of 6 ppm between the experimental and DFT values for free benzene. Thus, the comparison of the results of the calculations with experiment shows that there must be a low-to-modest pseudorotation barrier for the benzene ring to move around the metal.

Similar agreement between theory and experiment was found for the shifts assigned to $\mathbf{SI_1}$ and the spectator species, which is predicted by theory to be in equilibrium with the key intermediate $\mathbf{SI_2}$ (Figure 2). Theoretical modeling of $\mathbf{SI_2}$ led to the prediction of a very low concentration of this species relative to **SPEC** at equilibrium, as a consequence of its high reactivity. Moreover, the triplet (Table 3) of $\mathbf{SI_2}$ is slightly more stable than the singlet. If a singlet–triplet crossing did occur, it would be difficult to observe the triplet by NMR methods. In contrast, all of the other key species shown in Figure 1 were predicted to be lowest energy singlets and are consequently NMR-observable. Thus, although we observed the singlet **SPEC** species that forms from $\mathbf{SI_2}$, the low predicted equilibrium concentration of $\mathbf{SI_2}$ precludes observation by spectroscopic methods.

**Uniqueness of catalytic cycle for a solid-catalyzed reaction**: The catalytic cycle shown in Figure 1 is based on a foundation of both experimental and theoretical results.[20] The key to the rigorous elucidation of the catalytic intermediates is the near uniformity of the supported rhodium complexes, as demonstrated by the dynamic uniformity evidenced by $^{13}C$ NMR spectroscopy of the ethylene ligands in the supported as-synthesized complex **PRE**.[3]

In a more typical supported catalyst, exemplified by platinum particles supported on alumina, adsorption of acetylene led to a $^{13}C$ MAS NMR spectrum consisting only of a broad signal attributed to benzene at a shift close to the solution value.[22] Even when putative intermediates in surface catalysis are observed spectroscopically, they often prove to be spectator species present in low-energy states that are equilibrated with reactive species in the catalytic cycle. In the classic Wilkinson alkene hydrogenation cycle,[23] for example, such spectators dominate over the intermediates in the cycle.

In surface catalysis, there is a lack of observations of multiple reaction intermediates in any catalytic cycle. Such observations are especially challenging when the active sites are present at loadings of about 0.1 mmol g$^{-1}$ (as in our case) and in the absence of excess reactants to swamp the catalyst with one or another intermediate, as was done in Halpern's elucidation of the cycle for alkene hydrogenation by Wilkinson's complex in solution.[23]

  

## Conclusion

By selection of a crystalline support and a synthetic procedure by which the support replaces the anionic acac ligand of the precursor $[Rh(C_2H_4)_2(acac)]$, a single-site-supported bis-ethylene–$Rh^+$ catalyst precursor was prepared and characterized by EXAFS spectroscopy. Upon exchange of the ethylene ligands with acetylene, a catalytic cycle is initiated that operates in a molecularly precise manner, as in homogeneous catalysis. Well-defined intermediates in the catalytic cycle have been characterized by NMR spectroscopy. Theoretical modeling confirmed the experimental EXAFS and NMR results and was used to predict the full catalytic cycle, including transition states. The uniformity of the anchored catalyst and the precise characterization of the intermediates by experiment and theory have allowed a full characterization of the catalytic cycle.

## Experimental Section

**Synthesis of supported molecular catalyst**: The precursor state of the supported catalyst, **PRE**, was synthesized by slurrying a solution of $[Rh(C_2H_4)_2(acac)]$ (0.051 g, 0.20 mmol) in *n*-pentane (20 mL) with calcined dealuminated Y zeolite (with a Si/Al atomic ratio of 30; 2.0 g, 0.20 mmol) in a Schlenk flask at 200 K for 1 day. The solvent was removed by evacuation, and the resultant pale yellow powder, containing 1.0 wt% Rh (approximately one Rh atom per seven α-cages of the zeolite and approximately one Rh atom per five Al atoms), was stored in a glove box under nitrogen. The ethylene ligands in **PRE** exchanged readily with $[D_4]$ethylene or $[^{13}C_2]$ethylene on a vacuum line (as shown by IR and NMR spectra); several molecules of $[^{13}C_2]$acetylene could be adsorbed per $Rh^+$ site at 300 K.

**Acetylene cyclotrimerization catalysis in a flow reactor**: Charges (300 mg) of the as-synthesized form **PRE** were loaded into quartz reactors,[24] and pulses containing 2.8 acetylene molecules per $Rh^+$ site in a stream of helium carrier gas (650 mL min$^{-1}$) were delivered to the bed as the products were monitored by on-line GC-FID and GC-MS analysis (Agilent 6890 gas chromatograph and 5973 inert mass selective detector). Reactor temperatures of 413, 448, and 498 K were used in separate runs.

**Propylene hydrogenation catalysis in a flow reactor**: Hydrogenation of propylene was carried out at atmospheric pressure and temperatures ranging from 298 to 453 K by using a series of propylene pulses, each corresponding to 1.4 molecules per $Rh^+$, with a carrier gas stream of 5% $H_2$ in $N_2$ at a flow rate of 500 mL min$^{-1}$. This reaction was also carried out in a once-through plug-flow reactor with the supported catalyst (100 mg) at atmospheric pressure and 294 K with a total flow rate of 100 mL min$^{-1}$ with propylene (30 mbar) and $H_2$ (300 mbar) in He.

**Ethylene hydrogenation catalysis in a flow reactor**: Ethylene hydrogenation was carried out in a nearly isothermal, once-through plug-flow reactor with the as-synthesized catalyst (50 mg) at 294 K and atmospheric pressure. The reaction was carried out at steady state in a plug-flow reactor with a feed of $H_2$ (30 Torr), $C_2H_4$ (30 Torr), and He (700 Torr) and a feed flow rate of 100 mL min$^{-1}$. The products were analyzed with an on-line GC (Hewlett-Packard 5890), equipped with a 30 m × 0.53 mm DB-624 (J&W Scientific) capillary column and a FID. Conversions of ethylene to ethane were less than 5%, so that the reactor operated in the differential mode.

**Infrared spectroscopy**: A Bruker IFS 66v spectrometer with a spectral resolution of 4 cm$^{-1}$ was used to collect transmission IR spectra of powder samples in the form of pressed wafers. Samples were handled with exclusion of moisture and air. Each spectrum represents the average of 64 scans.

**NMR spectroscopy**: $^{13}C$ MAS and CP/MAS NMR spectra of the solid samples were acquired at 75 MHz with a Varian Infinity Plus spectrometer with an MAS spinning rate of 5.0 kHz. All sample spinning was done with nitrogen gas. The TOSS sequence[25] was used in some cases to suppress spinning sidebands and facilitate identification of isotropic peaks. Most spectra were acquired with samples at 298 K; essentially the same results were observed at temperatures as low as 240 K. Samples were prepared by loading the catalyst into a CAVERN apparatus[3] containing an MAS NMR rotor in a glove box. Upon sealing of the CAVERN, it was moved to a vacuum line and evacuated followed by adsorption of $[^{13}C_2]$acetylene measured by an MKS barotron gauge. The catalyst treated with labeled acetylene was then dropped into the NMR rotor and sealed with a Kel-F end cap before opening of the CAVERN to the atmosphere. All carbon spectra were referenced to hexamethylbenzene as an external standard whereby the methyl carbon signal was set to 17.35 ppm. For the CP acquisition of NMR spectra, a pulse delay of 0.5 s was used along with a spectral width of 50 kHz and a contact time of 2 ms. Each spectrum is the signal-averaged result of 2000 scans, which were processed with 20 Hz of exponential line broadening.

**X-ray absorption spectroscopy**: The X-ray absorption measurements were performed at beamline 2–3 at the Stanford Synchrotron Radiation Laboratory (SSRL) of the Stanford Linear Accelerator Center, Stanford, CA. The storage-ring electron energy was 3 GeV and the ring current was in the range of 80–100 mA. The as-synthesized material (with ethylene ligands, i.e., **PRE**) in a nitrogen-filled glove box was pressed into a thin wafer and loaded into an EXAFS cell;[26] the cell was evacuated to a pressure less than $1.3 \times 10^{-5}$ mbar and aligned in the X-ray beam. Spectra were collected in transmission mode at the Rh K edge with the sample at liquid-nitrogen temperature; 10 scans were recorded for the sample.

**Analysis of EXAFS data**: The X-ray absorption edge energy was calibrated with the measured signal of a rhodium foil (scanned simultaneously with the sample) at the Rh K-edge, which is represented as the inflection point at 23220 eV. The data were normalized by dividing the absorption intensity by the height of the absorption edge. Analysis of the EXAFS data was carried out with the software ATHENA of the IFEFFIT package and the software XDAP.[27] ATHENA was used for edge calibration, deglitching, data normalization, and conversion of the data into an EXAFS (chi) file. XDAP allowed the efficient application of a difference-file technique[28] for determination of optimized fit parameters.

The postulated models used in the data fitting included Rh–Rh, Rh–O, Rh–C, and Rh–Al contributions. Reference files, with backscattering amplitudes and phase shifts for Rh–Rh, Rh–Al, Rh–O and Rh–C contributions, were calculated with the software FEFF7.0[29] from crystallographic coordinates of the unit cells of the known reference compounds: Rh,[30] an Rh–Al alloy,[31] and $[Rh(C_2H_4)_2(acac)]$.[14]

Data analysis was carried out with unfiltered data; iterative fitting was performed until optimum agreement was attained between the calculated $k^0$-, $k^1$-, $k^2$- and $k^3$-weighted EXAFS data and the postulated model. The data were fitted in $r$ space with the Fourier-transformed $\chi(k)$ data ($r$ is distance from the absorbing atom, $\chi$ the EXAFS function, and $k$ the wave vector). The fitting ranges, determined by the data quality, were as follows: $k = 3.85$–$15.46$ Å$^{-1}$ and $r = 1.00$–$4.00$ Å (Supporting Information). The number of parameters used in fitting the data to each model (12 or 16) was always less than the estimated statistically justified number (23) computed with the Nyquist theorem.[32]

The approximate accuracies of the fit parameters are estimated to be as follows: coordination number $N$, ±20%; distance $R$, ±0.02 Å; Debye–Waller factor $\Delta\sigma^2$, ±20%; and inner potential correction $\Delta E_0$, ±20%. In some of the postulated models, the Rh–Al and Rh–Rh contributions are of questionable physical meaning (details are given in the Results section), and the errors in these contributions are larger than those stated immediately above.

**Electronic structure calculations**: Calculation of the potential-energy surfaces for acetylene cyclotrimerization was carried out for gas-phase $Rh^+$ complexes as well as zeolite-bound rhodium complexes. All calculations were done at the density functional theory (DFT) level. In the case of the zeolite-bound complexes, $AlO_4H_4^-$ was used to model the surface site on which the Rh atom was bound (with accompanying ligands). All DFT

  

electronic structure calculations for the singlet and triplet potential energy surfaces were carried out with the B3LYP exchange-correlation functional.[33] The Stuttgart relativistic effective core potential (ECP) and associated basis set were used for Rh,[34] and, for the other elements, the calculations were done with augmented correlation consistent polarized double zeta basis set (aug-cc-pVDZ).[35] These calculations were done with the Gaussian program system[36] on Cray XD-1 and SGI Altix computers at the Alabama Supercomputing Center.

In addition, the calculated structures determined with the larger zeolite cluster model incorporating eight tetrahedral sites (Figures 1 and 2) were optimized with the B3LYP exchange-correlation functional and the DZVP2 basis set[37] for the C, H, and O and the above-mentioned ECP and basis set for Rh. This larger zeolite cluster model has been extensively applied in calculations of spectroscopic properties of chemisorbed species in zeolites.[38] The basic structure defining the interaction of the $Rh^+$ with the zeolite site does not depend significantly on the size or form of the model of the zeolite site.

The theoretical chemical shifts shown in Figure 2 were computed by using the GIAO formalism[39] at B3LYP with the polarized triple-zeta basis set from Ahlrichs[40] and the Stuttgart ECP and basis set on Rh at a single geometry. The basis set from the Ahlrichs group has been shown to be very useful for the calculation of magnetic parameters for aiding the interpretation of NMR and EPR experiments.[41] For the GIAO calculations, the Stuttgart basis set was augmented by two sets of f and one set of g functions.[42] Values shown in Figure 2 are averages of isotropic shifts for carbon atoms involved in rapid fluxional processes. In the case of the benzene complex $\mathbf{SI_3}$, for example, six isotropic shifts were predicted at values between 68.0 and 148.2 ppm, and the average value due to exchange, predicted to be 100.0 ppm, is that shown in Figure 2. These calculations were done with computing time granted by the University of Southern California High Performance Computing Center and on the Cray XD1 at the Alabama Computing Center.

## Acknowledgements

The research at the University of Southern California was supported by the U.S. Department of Energy (DOE) grant DE-FG02-04ER15598, that at the University of California by DOE grant DE-FG02-04ER15600, and that at the University of Alabama by DOE grant DE-FG02-03ER15481 and the DOE-sponsored catalysis center through the Pacific Northwest National Laboratory. We acknowledge beam time and the support of the DOE Division of Materials Sciences for its role in the operation and development of beamline 2–3 at the Stanford Synchrotron Radiation Laboratory.

[1] a) S. Bhaduri, D. Mukesh, *Homogeneous Catalysis Mechanisms and Industrial Applications*, Wiley-Interscience, New York, **2000**, p. 239; b) R. H. Crabtree, *The Organometallic Chemistry of the Transition Metals*, 3rd ed., Wiley, New York, **2001**, p. xv, 534; c) D. B. Jacobson, G. D. Byrd, B. S. Freiser, *J. Am. Chem. Soc.* **1982**, *104*, 2320–2321.

[2] a) J. Guzman, B. C. Gates, *Dalton Trans.* **2003**, 3303–3318; b) J. C. Fierro-Gonzalez, S. Kuba, Y. L. Hao, B. C. Gates, *J. Phys. Chem. B* **2006**, *110*, 13326–13351; c) M. Tada, Y. Iwasawa, *Chem. Commun.* **2006**, 2833–2844; d) A. Corma, *Catal. Rev. Sci. Eng.* **2004**, *46*, 369–417.

[3] J. O. Ehresmann, P. W. Kletnieks, A. J. Liang, V. A. Bhirud, O. P. Bagatchenko, E. J. Lee, M. Klaric, B. C. Gates, J. F. Haw, *Angew. Chem.* **2006**, *118*, 588–590; *Angew. Chem. Int. Ed.* **2006**, *45*, 574–576.

[4] A. J. Liang, V. A. Bhirud, J. O. Ehresmann, P. W. Kletnieks, J. F. Haw, B. C. Gates, *J. Phys. Chem. B* **2005**, *109*, 24236–24243.

[5] A. M. Argo, J. F. Odzak, F. S. Lai, B. C. Gates, *Nature* **2002**, *415*, 623–626.

[6] R. Wesendrup, H. Schwarz, *Organometallics* **1997**, *16*, 461–466.

[7] H. P. Fritz, J. Manchot, *J. Organomet. Chem.* **1964**, *2*, 8–14.

[8] a) H. Werner, G. Canepa, K. Ilg, J. Wolf, *Organometallics* **2000**, *19*, 4756–4766; b) R. P. Hughes, A. S. Kowalski, B. T. Donovan, *J. Organomet. Chem.* **1994**, *472*, C18–C20.

[9] H. C. Foley, S. J. Decanio, K. D. Tau, K. J. Chao, J. H. Onuferko, C. Dybowski, B. C. Gates, *J. Am. Chem. Soc.* **1983**, *105*, 3074–3082.

[10] a) B. K. Teo, D. C. Joy, *EXAFS Spectroscopy, Techniques and Applications*, Plenum, New York, **1981**, p. viii, 275; b) E. D. Crozier, A. J. Seary, *Can. J. Phys.* **1980**, *58*, 1388–1399.

[11] Moreover, an attempt to fit the data with a Rh–Rh contribution with a distance of 3.1 Å was not successful (this is a typical distance between Rh atoms in dimeric complexes with bridging ligands and no Rh–Rh bonds[12]). This result is consistent with the difficulty of having bridged structures with two $Rh^+$ species close to each other in the zeolite; this situation would require two $Al(OSi)^-$ sites adjacent to each other, in violation of Löwenstein's rule regarding zeolite structures, and especially unlikely in zeolites with high Si/Al ratios such as ours.

[12] a) M. Abou Rida, J. Saikaili, A. K. Smith, A. Thozet, *Acta Crystallogr. Sect. C* **2001**, *57*, 352–353; b) L. Walz, P. Scheer, *Acta Crystallogr. Sect. C* **1991**, *47*, 640–641; c) J. Coetzer, G. Gafner, *Acta Crystallogr. Sect. B* **1970**, *26*, 985–991.

[13] H. H. Lamb, B. C. Gates, H. Knözinger, *Angew. Chem.* **1988**, *100*, 1162–1180; *Angew. Chem. Int. Ed. Engl.* **1988**, *27*, 1127–1144.

[14] M. Bühl, M. Håkansson, A. H. Mahmoudkhani, L. Öhrström, *Organometallics* **2000**, *19*, 5589–5596.

[15] H. Y. Afeefy, J. F. Liebman, S. E. Stein, "Neutral Thermochemical Data" in *NIST Chemistry WebBook*, *NIST Standard Reference Database Number 69* (Eds.: P. J. Linstrom, W. G. Mallard), National Institute of Standards and Technology, Gaithersburg MD 20899 (http://webbook.nist.gov), June **2005**.

[16] C. E. Moore, *Atomic Energy Levels as Derived from the Analysis of Optical Spectra*, *Volume III. Mo to La*, *Hf to Ac*, U.S. National Bureau of Standards Circular 467, Commerce, U.S.D.o., National Technical Information Service, COM-72-50283, Washington, D.C., **1971**.

[17] a) C. Sosa, J. Andzelm, B. C. Elkin, E. Wimmer, K. D. Dobbs, D. A. Dixon, *J. Phys. Chem.* **1992**, *96*, 6630–6636; b) N. Matsuzawa, J. Seto, D. A. Dixon, *J. Phys. Chem. A* **1997**, *101*, 9391–9398.

[18] J. H. Hardesty, J. B. Koerner, T. A. Albright, G. Y. Lee, *J. Am. Chem. Soc.* **1999**, *121*, 6055–6067.

[19] L. F. Veiros, G. Dazinger, K. Kirchner, M. J. Calhorda, R. Schmid, *Chem. Eur. J.* **2004**, *10*, 5860–5870.

[20] The use of density functional theory for determination of catalytic cycles taking place on surfaces has been illustrated by a number of researchers;[21] what sets our work apart from theirs is the demonstration of uniformity of the surface catalytic sites.

[21] a) E. Kukulska-Zajac, P. Kozyra, J. Datka, *Appl. Catal. A* **2006**, *307*, 46–50; b) M. Neurock, S. A. Wasileski, D. Mei, *Chem. Eng. Sci.* **2004**, *59*, 4703–4714; c) K. Honkala, A. Hellman, I. N. Remediakis, A. Logadottir, A. Carlsson, S. Dahl, C. H. Christensen, J. K. Nørskov, *Science* **2005**, *307*, 555–558.

[22] M. J. Lambregts, E. J. Munson, A. A. Kheir, J. F. Haw, J. F. *J. Am. Chem. Soc.* **1992**, *114*, 6875–6879.

[23] a) J. Halpern, T. Okamoto, A. Zakhariev, *J. Mol. Catal.* **1977**, *2*, 65–68; b) J. P. Collman, L. S. Hegedus, J. R. Norton, R. G. Finke, *Principles and Applications of Organotransition Metal Chemistry*, University Science Books, Mill Valley, CA, **1980**, pp. 334–338.

[24] D. M. Marcus, K. A. McLachlan, M. A. Wildman, J. O. Ehresmann, P. W. Kletnieks, J. F. Haw, *Angew. Chem.* **2006**, *118*, 3205–3208; *Angew. Chem. Int. Ed.* **2006**, *45*, 3133–3136.

[25] W. T. Dixon, J. Schaefer, M. D. Sefcik, E. O. Stejskal, R. A. Mckay, *J. Magn. Reson.* **1982**, *49*, 341–345.

[26] R. E. Jentoft, S. E. Deutsch, B. C. Gates, *Rev. Sci. Instrum.* **1996**, *67*, 2111–2112.

[27] a) M. Newville, *J. Synchrotron Radiat.* **2001**, *8*, 322–324; b) M. Vaarkamp, J. C. Linders, D. C. Koningsberger, *Phys. B* **1995**, *209*, 159–160.

[28] a) J. B. A. D. van Zon, D. C. Koningsberger, H. F. J. van't Blik, D. E. Sayers, *J. Chem. Phys.* **1985**, *82*, 5742–5754; b) P. S. Kirlin, F. B. M.

  

van Zon, D. C. Koningsberger, B. C. Gates, *J. Phys. Chem.* **1990**, *94*, 8439–8450.
[29] S. I. Zabinsky, J. J. Rehr, A. Ankudinov, R. C. Albers, M. J. Eller, *Phys. Rev. B* **1995**, *52*, 2995–3009.
[30] H. P. Singh, *Acta Crystallogr. Sect. A* **1968**, *24*, 469–471.
[31] J. D. H. Donnay, H. M. Ondik, *Crystal Data Determinative Tables, Vol. II*, National Bureau of Standards and the Joint Committee on Powder Diffraction Standards, Washington, DC, **1973**, p. C-4.
[32] F. W. Lytle, D. E. Sayers, E. A. Stern, *Phys. B* **1989**, *158*, 701–722.
[33] a) R. G. Parr, W. Yang, *Density-Functional Theory of Atoms and Molecules*, Oxford University Press, New York, **1989**; b) D. Becke, *J. Chem. Phys.* **1993**, *98*, 5648–5652; c) C. T. Lee, W. T. Yang, R. G. Parr, *Phys. Rev. B* **1988**, *37*, 785–789.
[34] W. Kuchle, M. Dolg, H. Stoll, H. Preuss, *J. Chem. Phys.* **1994**, *100*, 7535–7542.
[35] a) R. A. Kendall, T. H. Dunning, R. J. Harrison, *J. Chem. Phys.* **1992**, *96*, 6796–6806; b) T. H. Dunning, *J. Chem. Phys.* **1989**, *90*, 1007–1023.
[36] M. J. Frisch, G. W. Trucks, H. B. Schlegel, G. E. Scuseria, M. A. Robb, J. R. Cheeseman, J. A. Montgomery, Jr., T. Vreven, K. N. Kudin, J. C. Burant, J. M. Millam, S. S. Iyengar, J. Tomasi, V. Barone, B. Menucci, M. Cossi, G. Scalmani, N. Rega, G. A. Petersson, H. Nakatsuji, M. Hada, M. Ehara, K. Toyota, R. Fukuda, J. Hasegawa, M. Ishida, T. Nakajima, Y. Honda, O. Kitao, H. Nakai, M. Klene, X. Li, J. E. Knox, H. P. Hratchian, J. B. Cross, V. Bakken, C. Adamo, J. Jaramillo, R. Gomperts, R. E. Stratmann, O. Yazyev, A. J. Austin, R. Cammi, C. Pomelli, J. W. Ochterski, P. Y. Ayala, K. Morokuma, G. A. Voth, P. Salvador, J. J. Dannenberg, V. G. Zakrzewski, S. Dapprich, A. D. Danniels, M. C. Strain, O. Farkas, D. K. Malick, A. D. Rabuck, K. Raghavachari, J. B. Foresman, J. V. Ortiz, Q. Cui, A. G. Baboul, S. Clifford, J. Cioslowski, B. B. Stefanov, G. Liu, A. Liashenko, P. Prishkorz, I. Komaromi, R. L. Martin, D. J. Fox, T. Keith, M. A. Al-Laham, C. Y. Peng, A. Nanayakkara, M. Challacombe, P. M. W. Gill, B. Johnson, W. Chen, M. W. Wong, C. Gonzalez, J. A. Pople, Gaussian 03, Revision C.02, Gaussian, Inc. Wallingford, CT, **2004**.
[37] N. Godbout, D. R. Salahub, J. Andzelm, E. Wimmer, *Can. J. Chem.* **1992**, *70*, 560–571.
[38] a) M. S. Stave, J. B. Nicholas, *J. Phys. Chem.* **1995**, *99*, 15046–15061; b) J. O. Ehresmann, W. Wang, B. Herreros, D. P. Luigi, T. N. Venkatraman, W. G. Song, J. B. Nicholas, J. F. Haw, *J. Am. Chem. Soc.* **2002**, *124*, 10868–10874; c) P. W. Kletnieks, J. O. Ehresmann, J. B. Nicholas, J. F. Haw, *ChemPhysChem* **2006**, *7*, 114–116.
[39] K. Wolinski, J. F. Hinton, P. Pulay, *J. Am. Chem. Soc.* **1990**, *112*, 8251–8260.
[40] A. Schäfer, H. Horn, R. Ahlrichs, *J. Chem. Phys.* **1992**, *97*, 2571–2577.
[41] a) H. Cho, A. R. Felmy, R. Craciun, J. P. Keenum, N. Shah, D. A. Dixon, *J. Am. Chem. Soc.* **2006**, *128*, 2324–2335; b) Y. L. Gao, A. L. Focsan, L. D. Kispert, D. A. Dixon, *J. Phys. Chem. B* **2006**, *110*, 24750–24756.
[42] J. M. L. Martin, A. Sundermann, *J. Chem. Phys.* **2001**, *114*, 3408–3420.

Received: May 11, 2007
Published online: August 8, 2007

  